Taylor & Francis
Taylor & Francis Group

Transactions of the IMF

The International Journal of Surface Engineering and Coatings

ISSN: 0020-2967 (Print) 1745-9192 (Online) Journal homepage: https://www.tandfonline.com/loi/ytim20

Development of pore functionally graded Ti6Al4V scaffolds with biocompatible surface for bone repair

E. Shahimoridi, S. M. Kalantari & A. Molaei

To cite this article: E. Shahimoridi, S. M. Kalantari & A. Molaei (2019) Development of pore functionally graded Ti6Al4V scaffolds with biocompatible surface for bone repair, Transactions of the IMF, 97:5, 254-260, DOI: 10.1080/00202967.2019.1644768

To link to this article: https://doi.org/10.1080/00202967.2019.1644768

Published online: 27 Aug 2019.

TRANSACTIONS OF THE IMF
2019, VOL. 97, NO. 5, 254–260
https://doi.org/10.1080/00202967.2019.1644768

Development of pore functionally graded Ti6Al4V scaffolds with biocompatible surface for bone repair

E. Shahimoridi[a], S. M. Kalantari[a] and A. Molaei[b]

[a]Biomaterials Group, Department of Metallurgy and Materials Engineering, Iran University of Science and Technology, Tehran, Iran; [b]Department of Materials Engineering, Tehran Science and Research Branch, Islamic Azad University, Tehran, Iran

ABSTRACT

Pore functionally graded scaffolds (PFGS) were successfully produced *via* the powder metallurgical space holder technique as a result of the evaporation of magnesium (Mg) particles. The arranged layers containing 20, 40, and 60 vol.% Mg particles were compacted and sintered. In addition, morphological and porosimetry studies were performed to determine an optimum structure. PFGSs were characterised for homogeneous distribution and low agglomeration of micro- and macro-pores. Optimum PFGSs contained 5–60% porosity with an average macro-pore size of about 100 µm. Finally, an hydroxyapatite (HA) nanoparticles coating (about 10 µm thickness) was uniformly deposited on PFGS by the sol–gel technique and analysed. PFGSs studied exhibited greatly improved biocompatibility, cyto-compatibility and cell attachment. HA coating augmented the cell proliferation rate of PFGS from 70% to 87% after 14 days incubation.

ARTICLE HISTORY
Received 18 March 2019
Accepted 7 July 2019

KEYWORDS
Porous functionally graded scaffold; magnesium; hydroxyapatite; coating; biocompatible surface

1. Introduction

Although bioceramics and polymeric biomaterials have been characterised with weak mechanical behaviour and insufficient biocompatibility, titanium (Ti) and its alloys with high corrosion resistance, excellent mechanical properties, and remarkable biocompatibility have been widely utilised as promising implants in biomedical applications.[1,2] Stress shielding is the main shortcoming of Ti and its alloys as bone replacements. Stress shielding occurs when part of the load is taken by implants and shielded from going to the bone. Based on Wolff's law, areas under lower load or stress will respond by decreasing the bone mass. Bone loss may lead to the loosening of failure of the implant. Minimising of damage to tissues adjacent to the implant has encouraged researchers to utilise porous structures as a solution for solving this problem.[3,4]

Since natural bone has a heterogeneous structure with a gradient porosity, porous functionally graded scaffolds (PFGSs) with arranged structures have been studied as a promising candidate for utilisation in orthopaedic applications.[5] Different designs have been used.[3–6] These structures can be decorated by high porosity in the inner part, like cancellous bone, and low porosity in the outer part, like cortical bone. Furthermore, applying hydroxyapatite (HA) nanoparticle coatings with high similarity in crystallography and chemical composition to the natural bone by some specific deposition techniques, such as sol–gel, can improve the bone compatibility of PFGSs.[4,5]

The powder metallurgy (PM) method with space holder technique has been widely utilised due to its considerable advantages: low cost, highly precise control of process variables, and pore size. The gradient porosity could be formed by using the layer-arranging method. The basic principle of this method is to synthesise both metallic powder and space holder material to achieve a green compact and then sinter it *via* a two-step heat treatment process.[3] Among space holders, magnesium (Mg) has been introduced due to great strength and stiffness, high modulus elasticity, and good chemical stability, and excellent reducing nature in the Ti matrix.[3,6–8]

Recently, the authors' group has conducted research on Ti-6Al-4V/Mg scaffolds containing different porosities and determined their promising properties.[9,10] In this current study, the main focus is to move forward and produce Ti-based PFGSs embedding controlled porosity contents and develop and investigate HA coating on PFGS.

The flow chart of the fabrication of Ti-based PFGSs and investigations is illustrated in Figure 1. Firstly, PFGSs have been fabricated *via* powder metallurgy method and studied. Secondly, to improve the similarity of produced structure with natural bone, HA nanoparticle coating was deposited by sol–gel technique on the pretreated PFGS. Finally, its biocompatibility, cell proliferation and non-cytotoxicity were studied and compared.

2. Experimental procedures

2.1. Materials

The following materials were purchased from Merck: Ti-6Al-4V, pure Mg, vinyl alcohol (PVA), $Ca(NO_3)_2 4H_2O$, P_2O_5, ethanol, and acetone.

2.2. PFGS preparation

Residual spring-like chips from the machining process of Ti-6Al-4V bars were ball-milled and used as the starting material described previously.[7,8]

After the ball-milling process, powders were sieved in the range of 45–90 µm and rinsed. Mg powder (>99%) as a spacer was sieved to achieve the powder range of 90–180 µm.

CONTACT A. Molaei arman.molaei@yahoo.com Department of Materials Engineering, Tehran Science and Research Branch, Islamic Azad University, Tehran 14778-93855, Iran

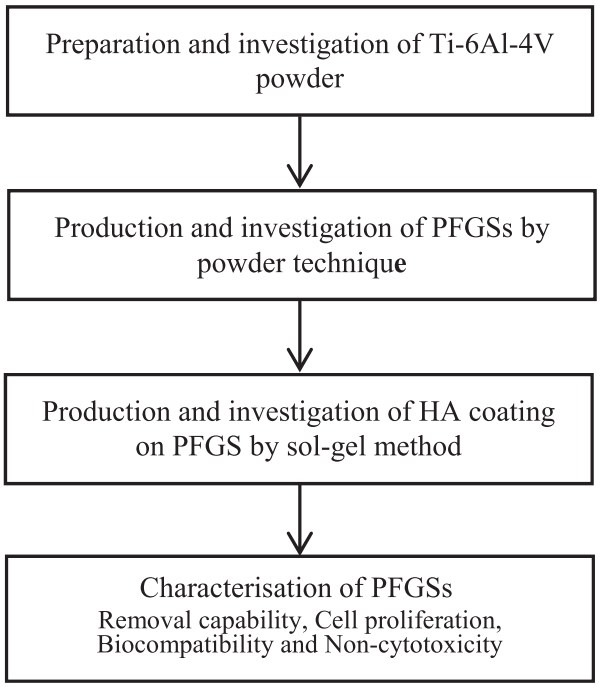

Figure 1. The flow chart of the production of Ti-based PFGSs and investigations.

PFGSs were produced by the PM method with the space holder technique. The first step is a layer-arranging process. In more detail, the layer arranging was performed at the first, second, and third layers containing 20, 40, and 60 vol.% of the space holder, respectively. At each layer, the relative ratio of Ti powder was synthesised with 5 wt.% PVA solution (5 wt.% PVA + 95 wt.% water) as the binder employed in an agate mortar. After synthesising, the arranged layers were uniaxially pressed at a pressure of 500 MPa in a steel die using a hydraulic press and then the green compact was weighed. The heat treatment was carried out under high purity Argon gas with a heating rate of 10°C min^{-1} up to 400°C for 3 h to debind the PVA and subsequently with a heating rate of 10°C min^{-1} up to 1100°C for 3 h to sinter the green compact and evaporate Mg powders, simultaneously. Finally, the PFGSs were cooled down to room temperature in a tube furnace and then weighed repeatedly.

2.3. Sol–gel coating

The surface of the PFGSs was pretreated by rinsing with acetone, ethanol, and deionised water and then dried. Hydroxyapatite (HA) nano-powders (<150 nm) were produced, as described previously.[1,2] HA coating was deposited on PFGSs *via* the sol–gel technique. In more detail, PFGSs were dipped into an HA solution for 1 min. After HA coating, they were aged at room temperature and then dried at 80°C. The heat treatment of PFGSs was performed in a tube furnace at 700°C for 5 h and then the PFGSs cooled.

2.4. Characterisation of PFGSs

2.4.1. Morphological study

Optical microscopy (KKmoon 640X student educational microscope) was used to observe the shape and size of the Ti-6Al-4V particles. Scanning electron microscopy (SEM: JEOL, JXA–840, Japan) was employed to study the type, size, and morphology of pores. The HA-coated PFGS was cold-mounted and its surface morphology and thickness were also assessed by SEM.

The quantitative elemental analysis of as-received Ti-6Al-4V bar and uncoated and HA-coated PFGSs was conducted by energy-dispersive X-ray spectrometry (EDX: JEOL, JXA-840, Japan). Elemental distribution analysis was studied on the cross-sectioned PFGS by elemental distribution mapping.

The structures of Ti-6Al-4V powder and HA-coated PFGS were analysed by X-ray diffraction (XRD: JEOL, JDX-8030, Japan) by continuous scanning at 40 kW over a range of 2θ angles from 5° to 80°.

Fourier transform infrared spectroscopy (FT-IR, Thermo Nicolet NEXUS 870 spectrometer) was performed on HA-coated PFGS in transmission mode in the mid-IR region of 400–4400 cm^{-1}.

2.4.2. Porosimetry

Archimedes' principle was utilised to determine the open porosity percentage of porous PFGSs according to ASTM B-328.[11] The procedure is as follow: Firstly, the dry weight (D_W) of PFGS was measured. PFGS was dipped into deionised water at 100° C for 2 h and measured as the dipped weight (I_W). Then, the PFGS was withdrawn from the water and immediately weighed (S_W). The open porosity percentage (P) was calculated according to the following formula:

$$\%P = \frac{S_W - D_W}{S_W - I_W} \times 100 \quad (1)$$

The measurements of shape, size, and distribution of pores of the PFGSs were also carried out by image analyser attached to an optical microscope and analysing software (Image Tool).

2.4.3. In-vitro study

2.4.3.1. Cell culture. After ultrasonically cleaning the PFGSs and drying, MG-63 human osteosarcoma cell lines (NCBI C-555) were cultured at a density of 1×10^4 cells on each sample. MG-63 cells were cultured in Dulbecco's modified eagle's medium supplemented with 10% fetal bovine serum, 100 IU mL^{-1} penicillin, and 100 µg mL^{-1} streptomycin. MG-63 cells were harvested with 0.25% trypsin-EDTA solution in phosphate buffered saline. MG-63 cells were incubated at 37°C in humidified air according to ISO 10993-5.

2.4.3.2. Cell attachment. MG-63 cells at a density of 5×10^3 cells per well in 24-well plates were placed on uncoated and HA-coated PFGSs. The plates were incubated at 37°C in humidified air. 2.5% glutaraldehyde buffered in 0.2 M phosphate-buffered saline was used for fixing cells after a 6 h incubation period. Graded alcohols were used for dehydrating samples. The morphology of the osteoblast cells attached to the PFGSs was observed by using SEM observation.

2.4.3.3. Cell proliferation assay. The proliferation rate of the osteoblast cells was assessed by employing dimethylthiazol diphenyl tetrazolium bromide (MTT) assay on uncoated and HA-coated PFGSs. Briefly, MG-63 cultured cells were suspended in the culture medium at a density of 1×10^3 cells per 50 µL and were added to each of the wells in the 96-microtiter plates. Plates were incubated at 37°C in a humidified atmosphere in air for 24 h. PFGSs were placed on MG-63 cells. One tissue culture polystyrene well was used as a control. The plates containing PFGSs and cells were incubated at 37°C with 5% CO_2 for 7 and 14 days. The role of the CO_2 existing in the incubated

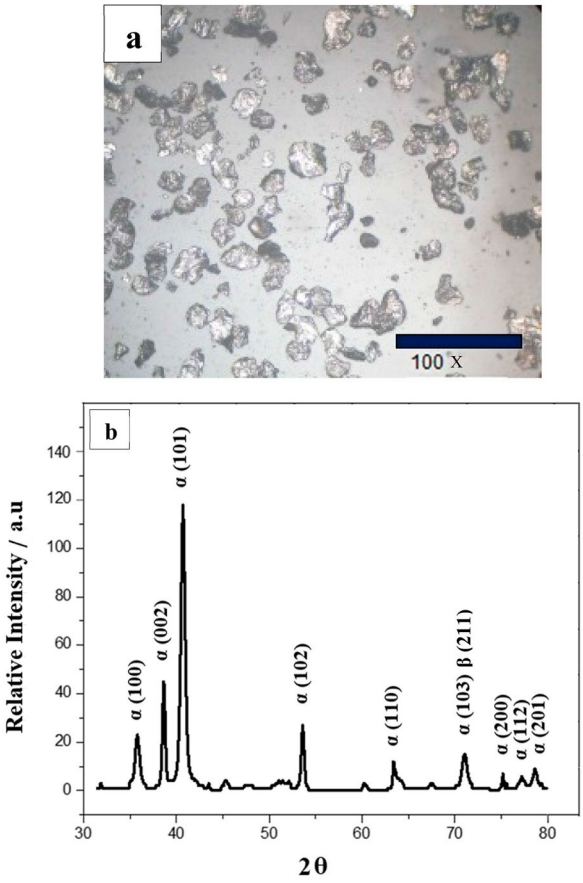

Figure 2. (a) Optical image at the magnification of 100x and (b) XRD pattern of Ti-6Al-4V powder.

area and changing to bicarbonate (HCO_3^-) is as a pH buffer to allow for nutrient and metabolites fluctuations without causing wild pH changes. At predetermined intervals, the PFGSs were taken out of the wells. 100 microlitres (μL) of MTT were added to each of the wells and incubated for another 4 h at 37°C. At this stage, the MTT was removed and the formazan crystals were dissolved by adding 100 μL of isopropanol in each well. The plates were placed in the incubator for 10 min and then in a cold room for 15 min prior to the absorbance measurement. Through Equations (2) and (3), the amount of toxicity % and viability % were determined.[12]

$$\text{Toxicity\%} = \left(1 - \frac{\text{Mean OD of sample}}{\text{Mean OD of control}}\right) \times 100 \quad (2)$$

$$\text{Viability\%} = 100 - \text{Toxicity\%} \quad (3)$$

3. Results and discussion

3.1. Characterisation of Ti-6Al-4V powder

Figure 2 displays the optical microscopy image of Ti-6Al-4V powder after the ball-milling process.

As is clear in Figure 2(a), Ti-6Al-4V powders are completely ball-milled. Ti based particles have irregular shapes with sharp points reflecting that the fabrication method is a mechanical technique characterised by cold-welded and fractured Ti based particles.[12] The chemical composition of the Ti-6Al-4V bar agrees with ASTM F1580-01 relating to Ti-6Al-4V powders used for medical implants (Table 1).[10]

XRD analysis of the Ti based powders is also presented in Figure 2(b).

As shown in Figure 2, the diffracted peaks of α- and β-crystalline structures relating to Ti-6Al-4V are determined. During the ball-milling process, some phenomena, such as releasing Ar gas, decreasing chamber temperature through the taking of rest time, and adding cooling liquid, prevent the oxidation of Ti powders.

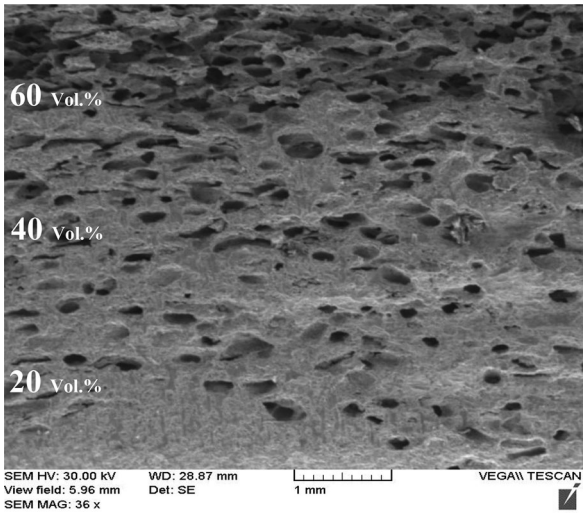

Figure 3. SEM micrograph of PFGSs using Mg particles.

3.2. Characterisation of porosity and pores

Typical SEM micrographs of PFGSs using Mg spacers are exhibited in Figure 3.

As expected and seen in Figure 3, an increase in the quantity of Mg spacers in PFGSs results in more total porosity contents. Apparently, by adding more Mg content, smoother pore surfaces with mostly spherical shapes and approximately the same dimensions, change to the stretched elliptical pores with different sizes relating to the irregular dimensions of Mg agglomerations and the deformation of pores achieved during the preparation process (Figure 3). Also, the porosity percentages of PFGSs are in the range of 5–60%.

As clearly elucidated in Figure 4, there are two types of pores: (i) macro-pores with rough cell walls, which are produced by the evaporation of Mg spacers, (ii) micro-pores in the cell walls and edges of the PFGSs, which are those left between Ti-6Al-4V powders. The sum of macro- and micro-pores constitutes the total porosity. The total amount of macro-porosity is enhanced with increasing Mg contents, whereas the micro-porosity content of PFGSs decreases since the volume occupied by cell walls and edges decreases.

As is observable in Figure 4, most of the macro-pores are in the range of up to 100 μm, while a few of the macro-pores have larger sizes than 100 μm. The formation of such large

Table 1. Mean chemical composition of Ti-6Al-4 V bar /wt.% compared to ASTM F1580-01.

Element	Ti	Al	V	Cu	Mo	Sn	Si	Fe	Zr	Mn	C
Sample	88.04	6.33	4.99	0.01	0.02	0.0	0.0	0.48	0.0	0.01	0.77
ASTM F1580-01	Balance	5.5–6.75	5.3–5.4	0.1	–	0.1	–	0.3	–	–	0.8

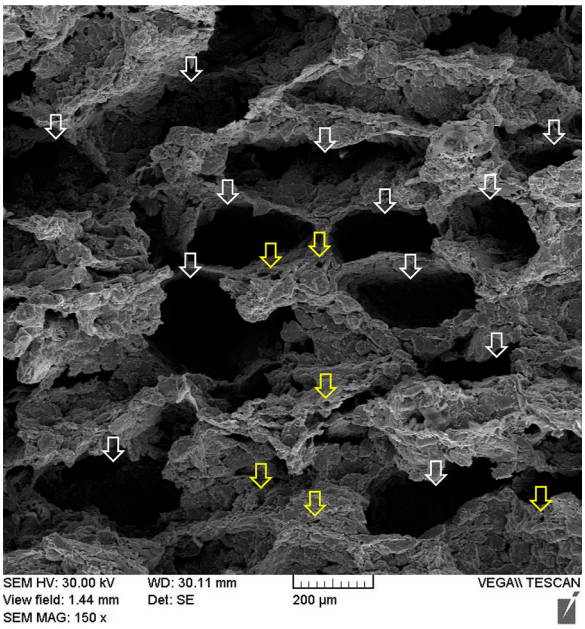

Figure 4. SEM micrograph of macro- and micro-pores in the third layer of PFGS using 60% Mg spacers (white arrows show macro-pores and yellow arrows show micro-pores).

pores is attributed to the coalescence of spacers, initial presence of agglomerations of spacers, smearing of partially sintered Ti-Al-4 V particles into the pores during metallographic sample preparation methods. Moreover, the size of micro-pores is generally lower than 10 µm.

In the case of studied PFGSs, pores are categorised in closed and open pores in the two first layers and the third layer, respectively (Figures 3 and 4). Archimede's analysis shows that these PFGSs have 37–44% open porosity.

It is also worth noting that the total porosity content for PFGS is found to be less than initial spacer contents, which may be related to the excessive shrinkage following the interconnection of macro-pores and the distortion of spacers during sintering.

3.3. Analysis of HA-coated PFGS

Figure 5 displays the top-view and cross-section images of HA-coated PFGSs using Mg spacers.

HA nano-particles deposit on Ti-6Al-4V PFGS by using appropriate calcination conditions (Figure 5(a)). As depicted in Figure 5(b), uniform thickness of HA coating (about 10 µm) with good adhesion to the substrate is produced. Aksakal and C. Hanyaloglu[13] reported that the optimum thickness of HA coating that leads to great biocompatibility is in the range of 10–20 µm.

EDS characterisation of the investigated area of the uncoated and HA-coated PFGS is shown in Figure 6.

The Ti, Al, and V peaks relate to Ti-6Al-4V. By comparing Figures 6(a and b), the appearance of Ca and P peaks verify the formation of HA coating on the substrate. A partial amount of Mg residue is detected in the uncoated PFGS indicating a good removal capability of space holders (Figure 6 (a)). The presence of Au and O peaks is attributed to the gold coating used to make the sample electrically conductive, and inefficient vacuum during SEM analysis.

Elemental distribution analysis of the coated PFGS is presented in Figure 7.

Obviously, Ca and P elements have high concentrations at the coating confirming the formation of a homogeneous HA coating. Lower Ca and P elements are noticeable in moving from the HA coating toward the substrate. The diffusion of Ca and P inside of the substrate and Ti element inside of the coating is also considerable in Figure 7.

Figure 8 plots XRD and FTIR patterns of HA-coated PFGS. Clearly, broad weak Ti and thin large HA peaks relate to Ti-6Al-4V PFGS and nanocrystalline coating, respectively, confirming the presence of these elements. There are chemicals such as titanium phosphate and calcium titanium phosphate exactly characterised by the HA peaks. Table 2 gives infrared absorption spectroscopy bond data of the coating formed on PFGS used Mg spacers. HA formation is also confirmed by FTIR results.

3.4. Biocompatibility properties

Figure 9 exhibits the morphology of the osteoblast cells cultured on coated and uncoated PFGSs using Mg spacers, analysed by SEM at different magnifications.

The MG-63 cells naturally lay over uncoated and coated PFGSs and have suitable stretching ability as well as normal morphology. Clearly, cells prefer to spread on both sides of the large gaps to bridge across the pores and provide closer surfaces for new born cells to attach to them. By comparing Figure 9(a and b), it is clearly distinguishable that HA

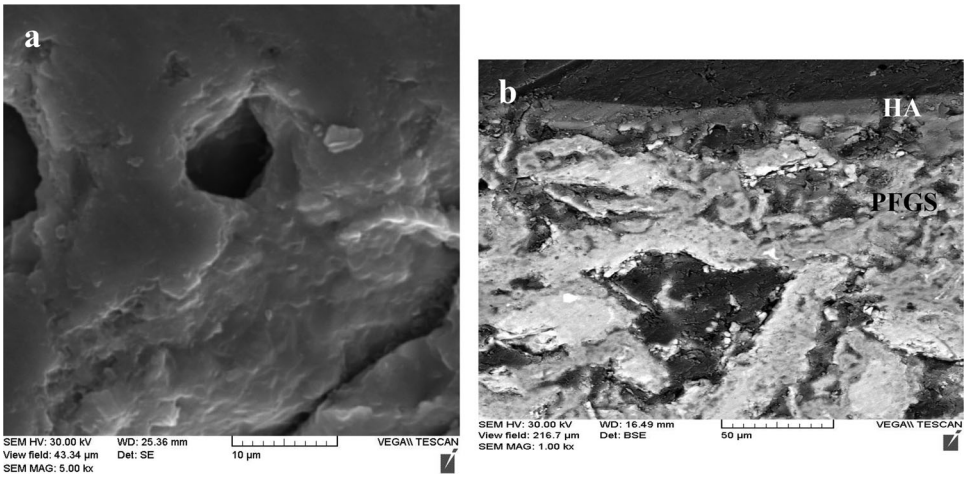

Figure 5. (a) Top-view and (b) cross-section of HA-coated PFGSs.

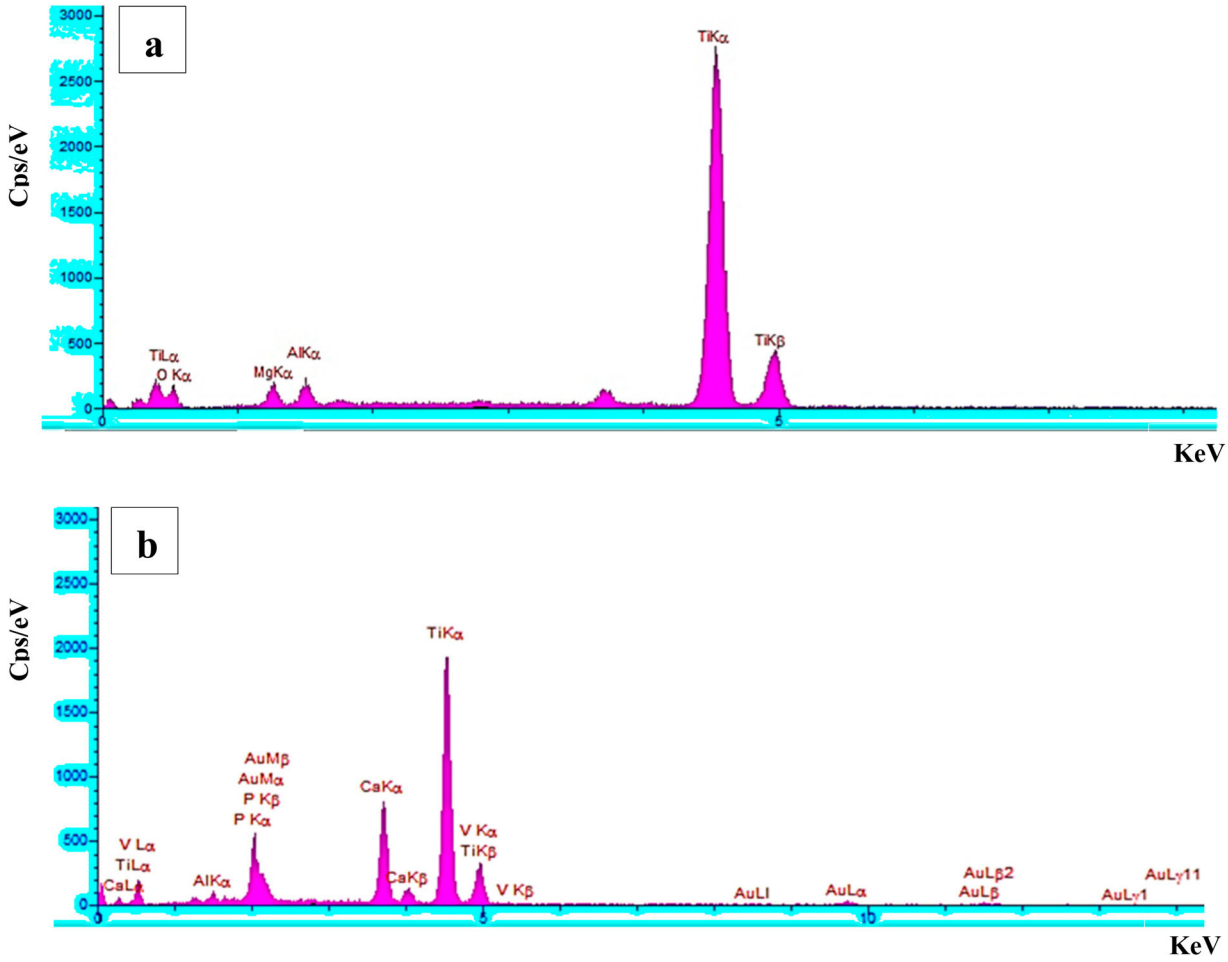

Figure 6. EDS of (a) uncoated PFGS and (b) HA-coated PFGS.

coating causes the higher distribution of MG-63 cells over PFGSs corresponding to its structural similarity with inorganic bone, reflecting that HA coating could improve the biocompatibility, cyto-compatibility, and cell attachment ability.

Interestingly, the shape and size of pores play important roles in improving biomedical properties since they facilitate the transportation of nutrients and oxygen inside PFGSs. It is believed that the minimum pore size for the growth of filamentous tissues, non-mineral bone tissues, and mineral ossification are 10–75, 75–100, and over 100 µm, respectively. Furthermore, during *in-vitro* and *in-vivo* experiments, the smaller and larger pore sizes achieve an augmented cell seeding and bone tissue regeneration, respectively.[10] Thus, due to embedding a wide range of pore size, such developed PFGSs can be considered as potential efficient implants for growing different tissues together in the biomedical area.

The cell proliferation can be evaluated from Equation (2). The results of MTT assay after 7 and 14 days incubation are presented in Figure 10.

As clearly illustrated, uncoated PFGSs show roughly 64% viability, while HA-coated PFGSs indicate more than 82% proliferation rate with respect to the control sample after 7 days incubation. By raising the incubation time to 14 days, these amounts reach 70% and 87% for uncoated and HA-coated PFGSs, respectively. With increasing the incubation time, cells have more chance of proliferation. What is more, in

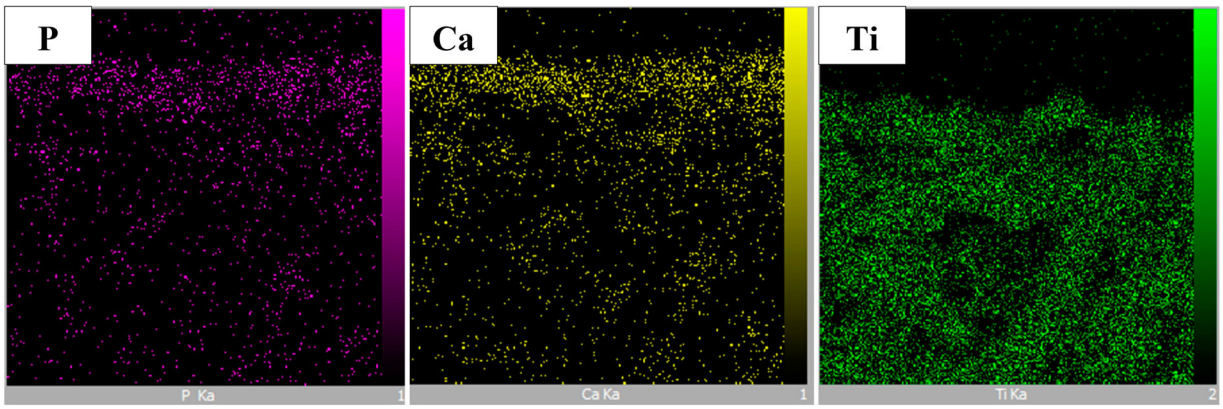

Figure 7. Elemental distribution analysis of P, Ca, and Ti element on PFGS.

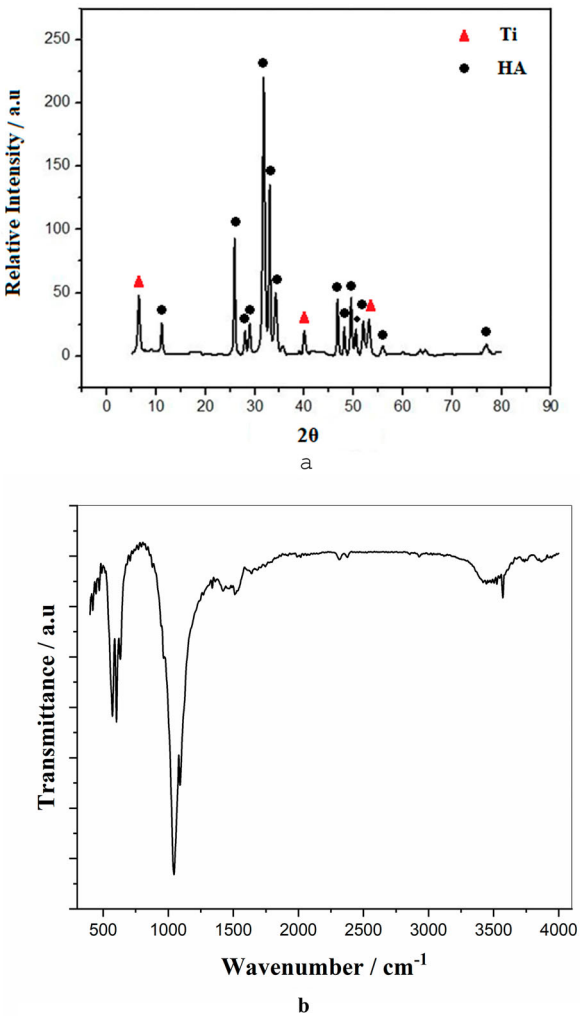

Figure 8. (a) XRD patterns for HA-coated PFGS and (b) FTIR spectra for HA coating.

Table 2. Infrared absorption spectroscopy of HA coating formed on PFGS.[1,2]

Wavenumbers/cm^{-1}	Type and group bond
587	P–O bond
627	O–H bond
1044, 1084	P–O bond
1413	C–O bond
3570	O–H bond

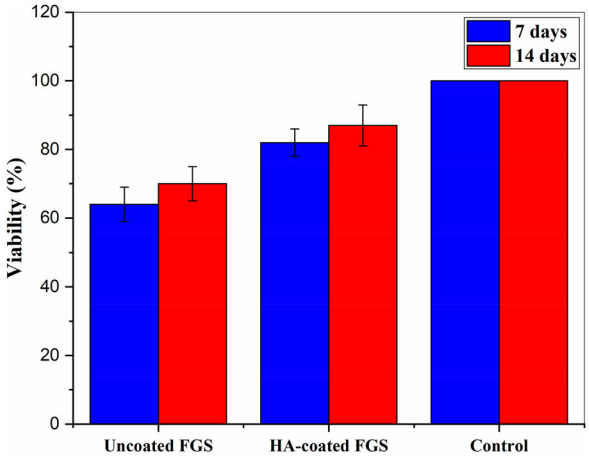

Figure 10. MG-63 cell proliferation of uncoated, coated, and controlled PFGSs determined by MTT after 7 and 14 days.

regard to inducing bioactivity, biocompatibility, and osteo-conductivity properties by HA coating, PFGSs with better cell proliferation distinguish themselves. Noticeably, the nano-size of HA characterises a higher surface-to-volume ratio, intensifying medical properties.[2]

More specifically, the remaining Mg, as pure Mg or a compound composition, in such PFGSs (as detected in Figure 6) is not harmful to the body since it stimulates the bone growth and subsequently mineralisation of the bone structure, as well as osteo-conductivity. Also, Mg element has a capability to dissolve in the body and form compounds which are non-toxic in small quantities.[14]

It is also remarkable to note that due to developing MG-63 cells during 7 and 14 days incubation, both PFGSs are non-toxic and possess appropriate abilities for supporting cultivated osteoblast cells, though more analysis is needed for verifying this discussion.

4. Conclusions

Nanocrystalline HA-coated Ti-6Al-4V PFGSs were successfully fabricated by powder metallurgical space holder technique as a result of the evaporation of Mg particles. Larger pores shapes and higher pore sizes were achieved in PFGSs by

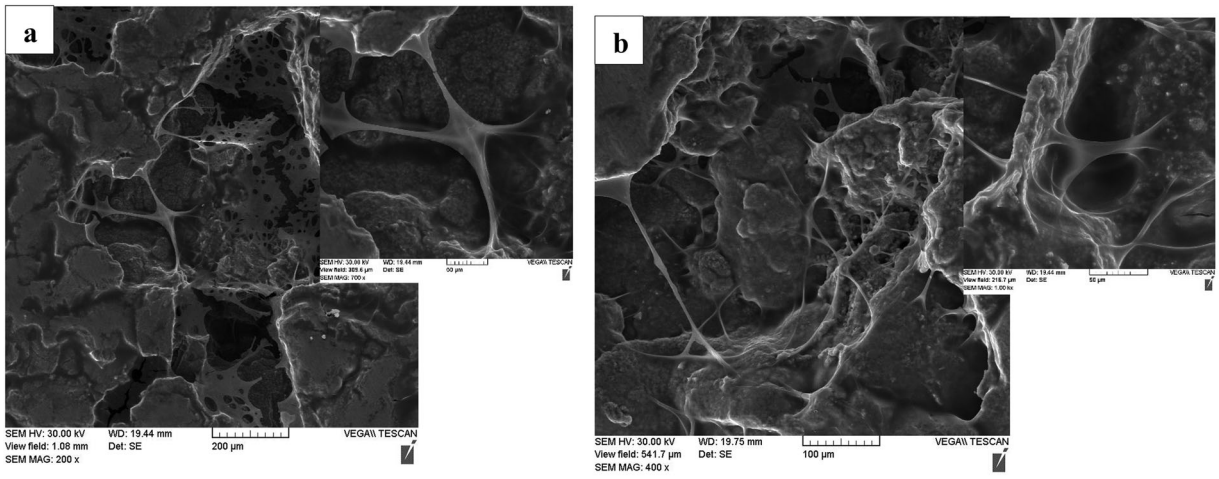

Figure 9. SEM micrograph of MG-63 cells attached to (a) uncoated and (b) HA-coated PFGS after 6 h.

using more Mg spacers. Also, uncoated and HA-coated PFGSs possessed great biocompatibility, cyto-compatibility, and cell attachment. Finally, HA-coated PFGSs had better cell proliferation rate than that of uncoated PFGSs and this rate was noticeably increased by extending incubation time.

Disclosure statement

No potential conflict of interest was reported by the authors.

References

1. A. Molaei, A. Amadeh, M. Yari and M. Reza Afshar: *Mater. Sci. Eng. C.*, 2016, **59**, 740–747.
2. A. Molaei and Y. Mardali: *Int. J. Polym. Mater.*, 2018, **68**, 701–713.
3. M. Ridzwan, I.Z. Solehuddin Shuib, A.Y. Hassan, A.A. Shokri and M.M. Ibrahim: *J. Med. Sci.*, 2007, **7**, 460–467.
4. R. Azari, H.R. Rezaie and A. Khavandi: *Ceram. Int.*, 2019. doi:10.1016/j.ceramint.2019.05.317.
5. A. Molaei, M. Yari and M.R. Afshar: *Appl. Clay. Sci.*, 2017, **135**, 75–81.
6. J. Hemant, G. Gupta, R. Kumar and D.P. Mondal: *Mater. Chem. Phys.*, 2019, **223**, 737–744.
7. S. Wang, L. Liu, K. Li, L. Zhu, J. Chen and Y. Hao: *Mater. Des.*, 2019, **168**, 107643.
8. A. Molaei, M. Yari and M.R. Afshar: *Ceram. Int.*, 2015, **41**, (10), 14537–14544.
9. S. M. Kalantari, H. Arabi, S. H. Mirdamadi and S. A. Mirsalehi: *J. Mech. Behav. Biomed. Mater.*, 2015, **48**, 183–191.
10. S. M. Kalantari, H. Arabi, SH. Mirdamadi and S. A. Mirsalehi: *Adv. Mater. Process.*, 2015, **3**, (2), 11–24.
11. ASTM, B. 328, Standard test method for density, oil content, and interconnected porosity of sintered metal structural parts and oil-impregnated bearing. ASTM International (2003). doi:10.1520/B0328-96R03E01.
12. P. Daswa, Z. Gxowa, M.J.I. Monareng and K. Mutombo: In IOP Conference Series: *Mater. Sci. Eng.*, 2018, **430**, (1), 012030.
13. B. Aksakal and C. Hanyaloglu: *J. Mater. Sci. Mater. Med.*, 2008, **19**, (5), 2097–2104.
14. X. Zhang, G. Zheng, J. Wang, Y. Zhang, G. Zhang, Z. Li, and Y. Wang: *J. Nanomater. - Special Issue on Biocompatibility and Toxicity of Nanobiomaterials*, 2013, **2013** (January), Article No. 18, 7 pages. doi:10.1155/2013/205076.